

Properties of monolayer solid helium and its melting transition

R. E. Ecke and J. G. Dash

Physics Department, University of Washington, Seattle, Washington 98195

(Received 28 February 1983; revised manuscript received 24 August 1983)

High-resolution heat-capacity measurements of ^4He adsorbed on exfoliated graphite have explored the incommensurate solid phase and its melting transition. The characteristics of the solid and the melting peaks resemble earlier measurements on Grafoil but the new results reflect greater uniformity of the present substrate, higher experimental resolution, and detailed substrate characterization. For temperatures $T < 0.06T_{\text{peak}}$ the Debye temperatures are independent of T , with values approximately equal to previous results. In the range $0.06T_{\text{peak}} < T < T_{\text{peak}}$ the heat capacity is increased by an exponential contribution attributed to the thermal activation of vacancies or dislocation pairs. Activation energies of the defects depend on density, and range from $20k_B$ to $27k_B$, in close agreement with nuclear-magnetic-resonance results and with estimates obtained from some computer-simulation studies. Peak temperatures are lower than the melting temperatures predicted by the theory of dislocation-mediated melting. Substrate characterization indicates variations in binding energy of 3.4×10^{-4} . These variations cause appreciable broadening of the melting peaks. We conclude that the experimental peaks are consistent with a first-order melting transition.

I. INTRODUCTION

The quantum systems of ^3He and ^4He adsorbed on the basal plane of graphite have been studied extensively with the use of calorimetric techniques,¹⁻⁵ neutron scattering,⁶⁻⁸ nuclear magnetic resonance,^{9,10} molecular beam scattering,¹¹ and volumetric vapor-pressure isotherms.^{12,13} The high-density region above 0.08 \AA^{-2} is of special interest due to the formation of a well-characterized crystalline two-dimensional (2D) solid¹ at low temperatures. At higher temperatures, there is a line of heat-capacity peaks whose peak positions increase in temperature as coverage increases. These peaks, measured by Hering *et al.*² for ^3He and by Bretz *et al.*¹ for ^4He on Grafoil, are associated with the melting of the incommensurate 2D helium solid. The order of the transition was not clear from those studies, though the transition appeared continuous based on the shapes of the experimental peaks.

The structure and melting of 2D solids have been the subject of numerous theoretical studies. Kosterlitz and Thouless¹⁴ and Feynman¹⁵ developed a theory of 2D melting based on the instability of the solid against the creation of dislocations. This theory was later extended by Halperin and Nelson and predicted a continuous transition.¹⁶ Chui¹⁷ has proposed an alternative mechanism for melting in which the formation of grain boundaries leads to a first-order melting transition. Computer simulations¹⁸ have also been used to study 2D melting. Some of these simulations have been interpreted as indicating first-order melting while others seem to show a continuous melting transition.

The applicability of the theories of 2D melting to adsorbed films is complicated by the structure imposed by the underlying substrate. The most suitable systems for testing the 2D melting theories in adsorbed films are incommensurate solid phases. ^4He /graphite provides such a system because the small size of the helium atoms relative to the substrate spacing makes the close-packed solid

phase highly incommensurate. Other attractive features of helium are as follows: (1) the solid is well described by a simple harmonic Debye model up to temperatures close to the melting temperature, (2) the solid phase and the solid-fluid phase boundary extend over a wide range of density and temperature, and (3) the low temperatures permit high resolution in the specific heat.

There are additional considerations when studying real experimental systems. The finite size of the substrate crystal domains can produce broadening of transitions which are sharp in the thermodynamic limit. Also, small variations in substrate binding energy have been shown to have appreciable influence on measured thermodynamic quantities.¹⁹

We have studied the high-density region of ^4He adsorbed on graphite foam, a graphite substrate with better uniformity than Grafoil. Section II describes the experimental details and specific-heat data. Sections III and IV present analysis of the specific-heat data, while Sec. V compares the results with theoretical predictions and other experiments.

II. HEAT CAPACITY

A. Adsorption cell and experimental method

The substrate used in this study was exfoliated graphite foam. The foam was machined into a cylinder, baked at 1400°C for several hours in purified flowing helium, forced into a gold-plated copper cell, and sealed with an indium *O*-ring cap. The compression of the foam and the gold-plated surface ensured good thermal contact. Heat was applied with a 1000- Ω Evanohm wire electric heater fastened to the cell with GE 7031 varnish. A 56- Ω Allen-Bradley carbon resistance thermometer measured the temperature of the cell; it was calibrated against a CryoCal²⁰ germanium thermometer. A thin-walled nylon tube provided structural stability and good thermal isolation for the cell.

The heat-capacity measurements were taken employing the adiabatic technique. In this technique a known amount of heat is introduced into the cell and the subsequent temperature change of the cell is measured; the preheat and postheat drift rates are then extrapolated to the midpoint of the heating interval to determine the average and the difference in temperature. An on-line mini-computer aided in the acquisition and processing of the specific-heat data. The heat capacity of the cell without adsorbed gas was measured, and this background signal was subtracted from the total heat capacity of both film and cell to give the contribution of the adsorbed gas.

The area of the cell was determined by a study of the $\sqrt{3}$ ordering transition of $^4\text{He}/\text{graphite}$.¹⁻⁵ The sharp specific-heat peaks of the order-disorder transition are used as an indication of the critical surface density, $n_c = 0.06367 \text{ \AA}^{-2}$. Although the value of the critical density obtained in this manner may differ from the actual critical density²¹ by about 1%, it provides a useful basis for intercomparison with previous studies where the area was calibrated in this way. With the use of this technique, the surface area of the foam cell is calculated to be 486.9 m^2 from a helium-gas dose of 115.7 cm^{-3} at STP. This yields a specific surface area of $29.7 \text{ m}^2/\text{g}$ for the 16.47-g foam sample. This value is in rough agreement with values obtained in other experiments^{5,22} on graphite foam.

B. Heat-capacity data

The $\sqrt{3}$ ordering transition was also studied to compare with previous heat-capacity measurements of ^4He on graphite foam. Figure 1 shows the specific-heat peak of a coverage close to the critical density compared with an analogous peak measured by Tejwani *et al.*⁵ The two curves are indistinguishable from each other over most of the temperature range, but differ slightly in the vicinity of the peak. This difference is due to the fact that in the peak region Tejwani used a finer temperature resolution (2 mK, as opposed to 4 mK in this study) so his maxima are

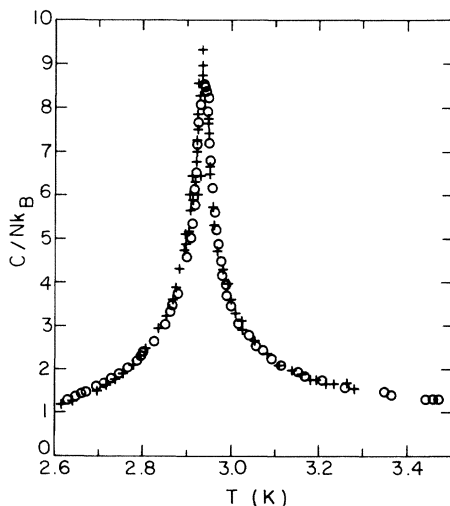


FIG. 1. Comparison of $^4\text{He}/\text{foam}$ specific-heat data of present study and Tejwani *et al.* (Ref. 5) for the order-disorder transition. The temperature scale of the Tejwani data has been shifted by + 8 mK.

slightly larger but the individual points have more scatter.

Heat-capacity measurements of seven different coverages of ^4He adsorbed on graphite foam were taken in the range $0.0842\text{--}0.09388 \text{ \AA}^{-2}$. From previous work by Bretz *et al.*,¹ the region from 0.078 to 0.115 \AA^{-2} is known to be a region of incommensurate 2D solid at low temperatures. The solid melts to a fluid phase at progressively higher temperatures as the density is increased. The density range of this study was chosen to avoid the effects of layer promotion and desorption which Elgin and Goodstein⁴ showed to be significant at the higher densities close to monolayer completion. Figure 2 shows a composite of the specific-heat data. The data points are omitted for the sake of greater clarity. All the data points of one heat-capacity curve are shown in Fig. 3, for the density of 0.08933 \AA^{-2} . This curve has a unique feature not seen in earlier work. Above the main peak, we now observe a smaller and broader peak centered at about 3 K. The height of this secondary peak is less than 0.03 above an extrapolated base line. The curves at higher density and the one at lower density do not exhibit a secondary peak. For the higher coverages this may be due to the appreciable increase in height of the main peaks. At about the same temperature increment (0.25 K) above the main peak, the curves bulge slightly. The temperature difference between the peak and this bulge appears to remain constant as density is increased, but the deviation becomes less visible as the main peak height increases and is undetectable at densities higher than 0.09167 \AA^{-2} .

The low-temperature phase has been identified as a 2D incommensurate solid by heat-capacity^{1,2} and neutron scattering^{6,8} measurements. Bretz *et al.*¹ found that the low-temperature specific heat has a quadratic temperature dependence, with Debye temperatures Θ_D that vary with density in a manner similar to bulk ^4He behavior. In the current study we also find this quadratic behavior of the low-temperature specific heat with values of Θ_D in good agreement with the previous measurements. In the present study we are particularly interested in the region at higher temperature, where the heat capacity deviates

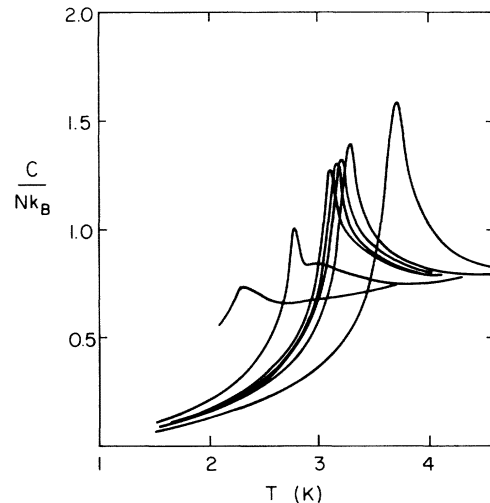


FIG. 2. Specific heat in the region of the incommensurate solid melting transition.

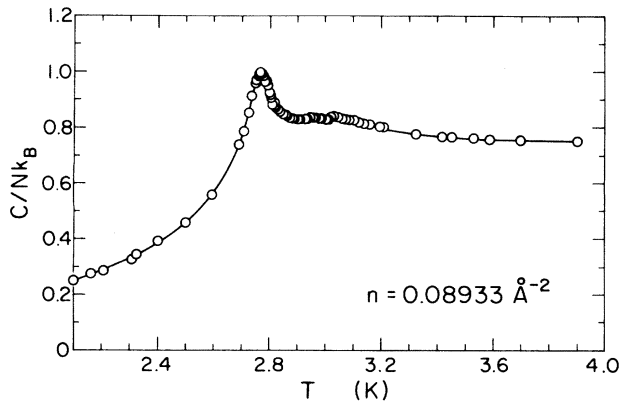


FIG. 3. Specific-heat data near melting, for the density $n=0.08933 \text{ \AA}^{-2}$.

from the quadratic law. For this reason we analyze the data in detail to measure and account for these deviations.

Our analysis is based on the two-dimensional Debye model, which has a heat capacity given by

$$\frac{C}{Nk_B} = 4(T/\Theta_D)^2 \int_0^{\Theta_D/T} \frac{x^3 e^x dx}{(e^x - 1)^2}. \quad (1)$$

In the low-temperature limit, $T \ll \Theta_D$, the specific heat approaches the quadratic form,

$$\frac{C}{Nk_B} = 28.848(T/\Theta_D)^2. \quad (2)$$

For bulk ^4He this low-temperature approximation is valid below $T/\Theta_D \cong 0.02$, while in 2D ^4He films on graphite the low-temperature behavior is seen to persist up to $T/\Theta_D \cong 0.07$. Values of Θ_D for the new foam data and for the previous Grafoil measurements are listed in Table I. For higher temperatures it is useful to express the heat-capacity data in terms of an effective temperature dependent $\Theta_D(T)$, calculated from Eq. (1) at each temperature. If one plots $\Theta_D(T)/\Theta_D(T=0)$ versus reduced temperature $T/\Theta_D(T=0)$ for all the coverages, the general behavior of the heat capacity and information about the density dependence of the frequency distribution can be seen. Figure 4 shows the data plotted in this way.

The density dependence of Θ_D can be expressed in terms of the Grüneisen parameter, $\gamma = d \ln \Theta_D / d \ln n$. A value of $\gamma = 4 \pm 0.1$ is obtained over the limited density range of the present study. Values for γ obtained from the data of Bretz *et al.* are in the range of 3.5–4.0 for densities between 0.09 and 0.105 \AA^{-2} .

TABLE I. Specific-heat data of the solid phase and melting transition for $^4\text{He}/\text{foam}$, $^4\text{He}/\text{Grafoil}$, (Ref. 1), and $^3\text{He}/\text{Grafoil}$ (Ref. 2).

	n (\AA^{-2})	Θ_D (K)	T_p (K)	T_p/Θ_D	C_p/Nk_B
$^4\text{He}/\text{Grafoil}^a$	0.0823	17.6	1.93	0.11	
	0.0873		2.65		0.73
	0.0927	26.7	3.12	0.117	1.11
	0.0942	29.8	3.65	0.122	1.38
	0.0967	33.0	4.18	0.125	1.55
	0.0991	37.6	4.7	0.125	1.71
	1.1037	42.2	5.8	0.135	2.12
	0.1079	47.8	6.8	0.142	5.2
	0.1134	53.9			
	0.1150	56.1	7.36	0.131	
$^4\text{He}/\text{Grafoil}^b$	0.078	14.5	1.2	0.083	
	0.082	17.4	2.0	0.115	
	0.084	21.3	2.25	0.108	0.6
	0.087		2.60		0.7
$^3\text{He}/\text{Grafoil}^b$	0.078	17.6	1.28	0.073	0.3
	0.079	17.9	1.48	0.083	0.4
	0.080	19.2	1.66	0.086	0.5
	0.082	21.1	1.97	0.093	0.7
	0.087	26.9	2.80	0.104	1.2
	0.092	33.7	3.74	0.111	1.6
	0.102	52.3			
$^4\text{He}/\text{foam}$	0.084 2		2.30		0.74
	0.089 33	25.1	2.77	0.110	1.00
	0.090 75	26.4	3.10	0.117	1.27
	0.090 99	26.7	3.15	0.118	1.30
	0.091 23	27.0	3.18	0.118	1.33
	0.091 67	27.5	3.27	0.119	1.39
	0.093 88	30.3	3.69	0.122	1.59

^aReference 1.

^bReference 2.

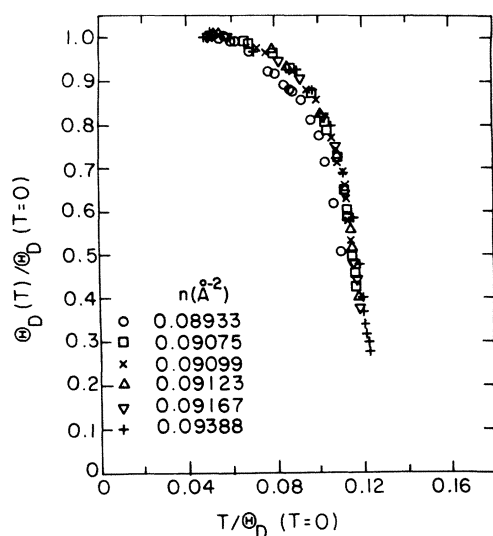


FIG. 4. $\Theta_D(T)/\Theta_D(T=0)$ vs $T/\Theta_D(T=0)$.

Since the Debye model fits quite well at low temperatures, it can be used to extrapolate the entropy at $T=0$ K. The film entropy is obtained by integrating the heat capacity,

$$\frac{S}{Nk_B} = 14.424(T_0/\Theta_D)^2 + \int_{T_0}^T \frac{C}{Nk_B T} dT, \quad (3)$$

where

$$T_0/\Theta_D < 0.06.$$

Figure 5 shows the entropy of the helium film. The entropy change on melting is obtained by evaluating the integral expression in Eq. (3) over the temperature interval of the specific-heat peak and subtracting an approximate baseline entropy. Values for $\Delta S_{\text{melt}}/Nk_B$ of 0.03 ± 0.005 for $n=0.08933 \text{ \AA}^{-2}$ to 0.08 ± 0.02 for $n=0.09388 \text{ \AA}^{-2}$ are obtained. The bulk-helium melting entropy per particle is about 0.5 at comparable interatomic spacing.²³

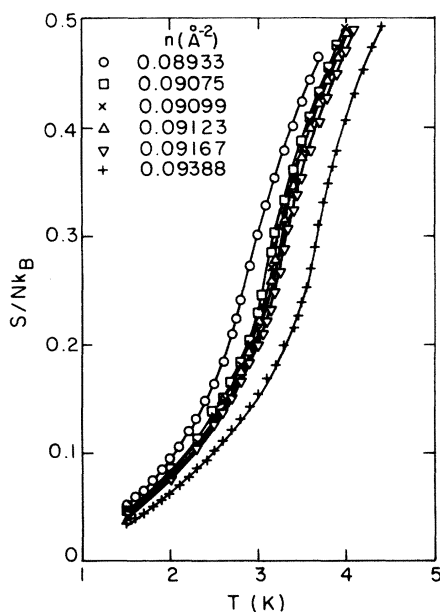


FIG. 5. Entropy obtained from integration of specific heat.

Heat-capacity isotherms have the distinct property that in regions of two-phase coexistence, C is linear in the total number of atoms. This is a necessary but not sufficient condition for the existence of two phases, since the heat capacity in certain single-phase regimes is predicted to vary linearly with density, although these phases are unlikely to be present in the density and temperature regions of interest to this study. Although the coverages are closely spaced to be able to distinguish a narrow two-phase region, the data are inadequate to reveal linear sections with breaks in slope at the ends that would indicate a difference between the coexistence region and the single-phase region. Either there is no coexistence or the two-phase region is too narrow to be delineated with the present data. The resultant limits on the width of any two-phase region are $\Delta T < 0.3 \text{ K}$ and $\Delta n < 0.001 \text{ \AA}^{-2}$.

In considering other features of the heat-capacity results obtained in this work it is constructive to compare them with earlier experiments. Table I shows a compilation of helium/graphite solid phase and melting parameters obtained from various specific-heat studies. Bretz *et al.*¹ and Hering *et al.*² studied the melting transition of ^4He adsorbed on Grafoil substrates. Bretz concentrated on the high-temperature behavior while Hering's data emphasized the low-temperature portion of the phase boundary. Results from both Grafoil studies agree quite well, but comparison with the current foam study indicates a sizable difference between their density-temperature phase boundaries and peak heights. Figure 6 shows two sets of data with comparable peak temperatures. The foam signals have an increased peak height of $\Delta C/Nk_B \cong 0.2$ over the corresponding Grafoil peaks. In Fig. 7(a), the phase boundary, as defined by the peak temperatures, is plotted. The curves seem to be uniformly shifted, with the exception of the Bretz peak at $n=0.0926 \text{ \AA}^{-2}$. If that peak is too high by 0.7%, then the uniform offset of the two curves is also about 0.7%. This is close to the error limits of the experimental determination of the surface density (about 0.5% for each study), and thus the deviations are likely a result of systematic error. A similar shift is observed in the density dependence of both the heat-capacity

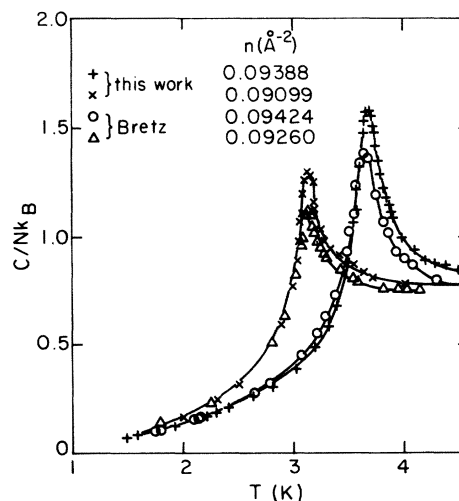


FIG. 6. Comparison of specific-heat melting peaks on graphite foam and on Grafoil.

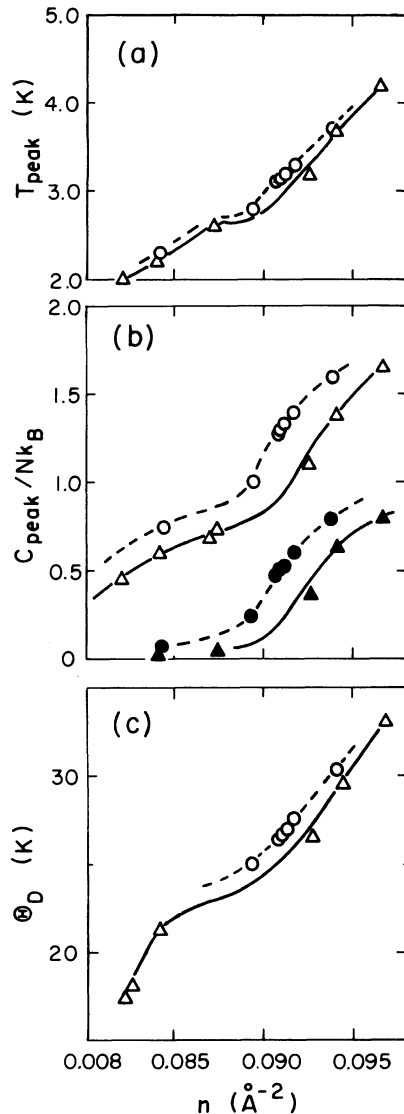


FIG. 7. (a) Specific-heat peak temperatures versus density for foam (\circ) and Grafoil (\triangle) substrates. (b) Specific-heat peak heights vs density for foam (\circ) and Grafoil (\triangle) substrates. Open symbols: full peak height. Solid symbols: baseline-subtracted peak height. (c) Specific-heat Debye temperatures vs density for foam (\circ) and Grafoil (\triangle) substrates.

peak heights [Fig. 7(b)] and the Debye temperatures [Fig. 7(c)]. The shift for the Debye temperatures is only slightly larger than the phase-boundary shift and is probably associated with the same systematic variations in density. The peak heights, on the other hand, show a clear increase for the foam data, as previously noted, even when the densities are adjusted to allow for the systematic shift.

A significant feature in the density dependences of $T_{\text{peak}}(n)$, $\Theta_D(n)$, and $C_{\text{peak}}(n)$ (Fig. 7) is the sudden increase in the slopes of the curves occurring at a density of about 0.089 \AA^{-2} . Other evidence for some fundamental effect occurring at that density is the anomalous dependence of the reduced Debye temperature on reduced temperature (Fig. 4) for the density $n=0.08993 \text{ \AA}^{-2}$. This density is also the one for which the broad secondary peak (Figs. 2 and 3) is clearly visible.

III. PROPERTIES OF THE SOLID PHASE

The low-temperature specific heat for coverages between 0.078 and 0.115 \AA^{-2} has the temperature dependence of a 2D Debye solid, but above $T/\Theta_D \cong 0.06$, the specific heat increases faster than the Debye specific heat. This increase is shown in Fig. 4, where the data are plotted in terms of $\Theta_D(T)/\Theta_D(T=0)$. In this section we will consider possible sources for the excess specific heat. One possible source might be contributions from a continuous melting transition but the temperature where the increase begins, $|T - T_c|/T_c = 0.5$, is far below the transition temperature, so contributions from that source should be small. Other possible sources of the increased specific heat are frequency dispersion due to the discrete nature of the lattice, anharmonicity, or the thermal activation of defects. We will discuss each of these in the following sections.

A. Frequency dispersion and anharmonicity

A source for the failure of the Debye expression and the increased specific heat is the neglect of the discrete nature of the lattice. The Debye approximation assumes that the lattice can be treated as an elastic continuum because only long-wavelength phonons contribute to the heat capacity at low temperatures. As soon as shorter-wavelength phonons are excited, the discrete nature of the lattice must be included. Goodstein and Greif²⁴ calculated the dispersion curves, $\omega(k)$, of the longitudinal and transverse modes of the 2D helium solid at $n=0.092 \text{ \AA}^{-2}$ along the two symmetry directions of the Brillouin zone. From these curves we have calculated the density of states $G(\omega)$ by constructing the constant- ω surfaces of both modes and by integrating the area in k space between closely spaced constant- ω surfaces to approximate the relation

$$G(\omega)d\omega = \int d^2k, \quad (4)$$

such that

$$\omega \leq \omega(\vec{k}) \leq \omega + d\omega.$$

It is only necessary to calculate the contribution from $\frac{1}{12}$ of the zone due to the symmetry of the triangular lattice.²⁵ Figure 8 shows the calculated $G(\omega)$, normalized to the $2N$

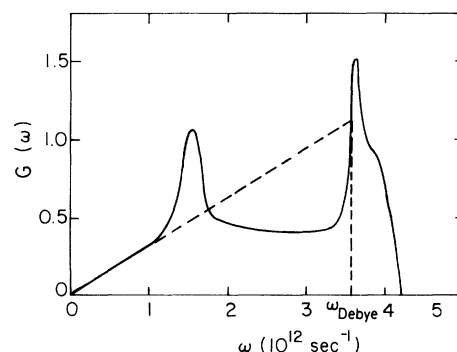


FIG. 8. Phonon frequency spectrum calculated from dispersion curves of Goodstein and Greif (Ref. 24). Debye spectrum is shown as dashed line.

modes of the lattice. The zone-boundary singularities are not visible, but the peaks at 1.5 and 3.7 (times 10^{12} rad/sec) show the distinct contributions from the transverse and longitudinal modes. Any low-temperature deviations from the Debye approximation (dashed line, Fig. 8) are dominated by the dispersion of the transverse mode.

Thermodynamic quantities of the solid are calculated as derivatives of the Helmholtz free energy per particle, $F(n, T)/N$, given in the harmonic approximation by

$$\frac{F(n, T)}{N} = -\epsilon_0 + u(n) + \frac{\hbar}{2} \int_0^\infty \omega G(\omega) d\omega + k_B T \int_0^\infty G(\omega) \ln(1 - e^{-\beta\hbar\omega}) d\omega, \quad (5)$$

where $u(n)$ is the static lattice energy per particle. Table II shows the results of the calculation of the specific heat, $C = -\partial^2 F / \partial T^2$, for the distribution calculated above. The heat capacities from the quadratic and Debye integral expressions are included for comparison. Figure 9 shows the calculation compared with the experimental data. At low temperature ($T/\Theta_D < 0.06$) the calculation predicts larger deviations from the Debye expression than are seen in the experimental results. In three dimensions the specific heat deviates from the Debye form close to the temperature predicted by a similar calculation,²⁶ but the 2D calculation predicts a breakdown of the Debye approximation at $T/\Theta_D \cong 0.03$, about half of the experimental value. The 2D lattice dynamics calculation cannot account for the much larger specific-heat deviation above $T/\Theta_D \cong 0.08$. The failure of the 2D calculation to predict the T^2 dependence of the experimental specific heat up to $T/\Theta_D \cong 0.07$ suggests that the calculated density of states is not accurate enough for this purpose.

The helium potential is highly anharmonic due to the large zero-point motion. However, the effective averaged potential gives rise to a solid which is well described in the harmonic approximation. In three dimensions $\Theta_D(T)/\Theta_D(T=0)$ for ^4He , and the classical rare gases argon and krypton are nearly the same at equal values of $T/\Theta_D(T=0)$.²⁷ This implies that in three dimensions, anharmonic contributions to the specific heat of ^4He are small and that the deviations from the Debye expression result from other sources. The increased range of validity of the Debye expression suggests that the effective anharmonicity is small in the helium film as well.

B. Thermal defect activation

In a solid, defects such as vacancies, interstitials, and dislocations are thermally activated in equilibrium concentrations that depend on the defect excitation energies. Certain defects are expected to be predominant due to their low relative activation energies. For example, in the rare-gas solids the interaction potential strongly favors vacancy formation rather than activation of interstitials.²⁸ Isolated dislocations cannot exist in an infinite system at low temperature because the elastic energy of a dislocation diverges with the size of the system. However, dislocation pairs have finite energy and are therefore excited at finite temperature. They are also observed in computer simulations of 2D melting.^{29,30} Other defects such as grain boundaries and disclinations are not expected to contribute at low temperature, although close to melting they may be important.^{16,31} In the three-dimensional (3D) rare-gas solids, vacancies are thought to be the primary thermally activated defect,^{26,28} but analysis of the specific-heat data is difficult because of the complex lattice contribution. In two dimensions one expects that vacancies and dislocation pairs are the most probable thermally activated defects; they have very similar structure when the dislocation pairs have a separation of one interatomic spacing.³¹

We have analyzed our data in terms of a thermal activation of noninteracting vacancies or unseparated dislocation pairs. As we cannot distinguish between these microscopic configurations, we will refer to them simply as defects. The lattice contribution to the specific heat is taken to be the Debye expression above $T/\Theta_D \cong 0.06$ so that the excess heat capacity ΔC is attributed to thermal activation. In the dilute-concentration limit, the heat capacity due to thermal activation is

$$C_d / Nk_B = (u_a / k_B T)^2 e^{-(u_a - Ts_a) / k_B T}, \quad (6)$$

and the fractional defect concentration is

$$N_d / N = e^{-(u_a - Ts_a) / k_B T}, \quad (7)$$

where u_a and s_a are the energy and entropy of activation per defect excitation at constant area, N_d is the number of defects, and N is the number of adsorbate atoms.²⁸ The quantities u_a and s_a are taken to be independent of temperature. Figure 10 shows $\ln[\Delta C(T/\Theta_D)^2]$ vs Θ_D/T .

TABLE II. Specific heat of ^4He /graphite from lattice dynamics calculation. $\Theta_D = 27.31$ K, $n = 0.092$ \AA^{-2} . C_Q equals the quadratic Debye approximation, C_D equals the integral Debye specific heat, and C_{LD} equals the lattice dynamics specific heat.

T (K)	T/Θ_D	C_Q/Nk_B	C_D/Nk_B	C_{LD}/Nk_B	$\Theta_D(T)/\Theta_D(T=0)$
0.20	0.007 31	0.001 54	0.001 54	0.001 54	1.0000
0.60	0.021 92	0.013 86	0.013 86	0.013 87	0.9996
1.0	0.035 3	0.038 51	0.038 51	0.039 03	0.9933
1.4	0.051 15	0.075 47	0.075 47	0.079 82	0.9724
1.8	0.065 76	0.124 76	0.124 75	0.137 86	0.9512
2.2	0.080 38	0.186 37	0.186 12	0.209 47	0.9422
2.6	0.094 99	0.260 30	0.258 79	0.289 26	0.9444
3.0	0.109 6	0.346 55	0.340 96	0.373 11	0.9532
3.4	0.124 22	0.445 13	0.429 97	0.458 44	0.9649

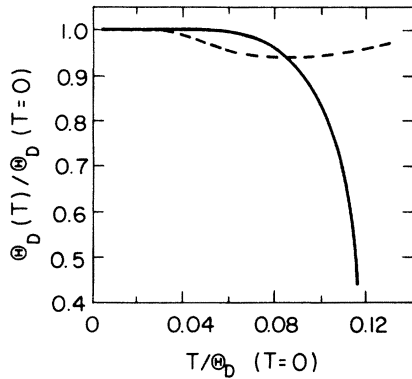


FIG. 9. Reduced Debye temperatures vs reduced temperature for measured heat capacities (—) and 2D lattice dynamics calculation (---).

Over the range $9.5 < \Theta_D/T < 12.5$, the data fall on a straight line, consistent with Eq. (6). Table III shows the empirical values of activation energy ($\pm 4\%$), activation entropy ($\pm 15\%$), and defect concentration at $T/\Theta_D = 0.11$. The small fraction of defects is consistent with the dilute-concentration approximation made in obtaining Eqs. (6) and (7).

The low-temperature ($\Theta_D/T > 13$) deviations apparent in Fig. 10 may be due to real corrections or to systematic errors in the heat-capacity data, but these errors are small. As can be seen in Fig. 11 the total specific heat is well represented up to $T/\Theta_D \cong 0.10$ by the sum of a lattice contribution with constant Θ_D and a vacancy activation term.

NMR results^{9,32} for ^3He /graphite also show an activation-energy form and were interpreted as due to vacancy excitation. The analysis just presented is constant with that description and agrees fairly well with the activation energies obtained in that work. At a coverage of $n = 0.0896 \text{ \AA}^{-2}$, the NMR results indicate $u_a/k_B = 21 \pm 2 \text{ K}$ while our measurements yield $u_a/k_B = 20.7 \pm 0.8 \text{ K}$ for nearly the same density ($n = 0.08933 \text{ \AA}^{-2}$). Although the systems are different helium isotopes, the evidence systematically points to defect formation in these 2D solid

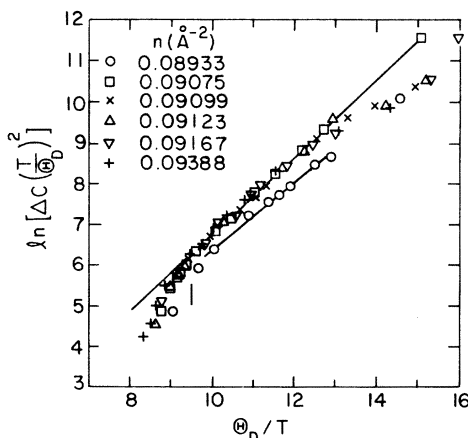


FIG. 10. Temperature dependence of the excess specific heat, $\Delta C = C_{\text{expt}} - C_{\text{Debye}}$.

TABLE III. Defect activation energies, entropies, and concentrations from specific heat of ^4He /foam.

n (\AA^{-2})	u_a/k_B (K) (± 1 K)	s_a/k_B (± 0.3)	N_d/N ($\times 10^{-3}$)
0.08933	20.7	2.2	5.2
0.09075	25.2	2.9	3.1
0.09099	24.4	2.6	3.3
0.09123	25.3	2.7	3.1
0.09167	24.9	2.5	3.1
0.09388	27.3	2.4	3.0

systems below the melting transition. The excitation value of $u_a/k_B = 40 \text{ K}$ reported by Lauter *et al.*³³ in a neutron scattering study of ^3He /Grafoil is of the same order of magnitude but the uncertainties in the neutron data are much larger than in the specific-heat and NMR measurements. We will discuss the neutron scattering results in more detail in Sec. V.

IV. HETEROGENEOUS EFFECTS ON A FIRST-ORDER MELTING TRANSITION

Above the region where thermal defect excitation is the primary excess specific heat, the heat capacity rises quickly to a peak previously identified as the melting of the 2D solid phase. The order of the transition has been thought to be continuous due to the rounded and symmetric features of the peaks. However, finite-size effects and the influences of variations in binding energy were not considered in making that identification. We now explore the possibility that the transition is intrinsically first order but that the heterogeneous properties of the real film broaden the ideal first-order peaks into the experimentally observed peaks. Continuous melting transitions are discussed in Sec. V.

The techniques discussed by Ecke *et al.*¹⁹ can be applied to get a quantitative estimate of the effects of energy heterogeneity on an ideal first-order melting transition. For an accurate calculation of these effects, one needs a complete thermodynamic description of the ideal system and the distribution of substrate binding energies. This is not possible with the specific-heat data and the characteri-

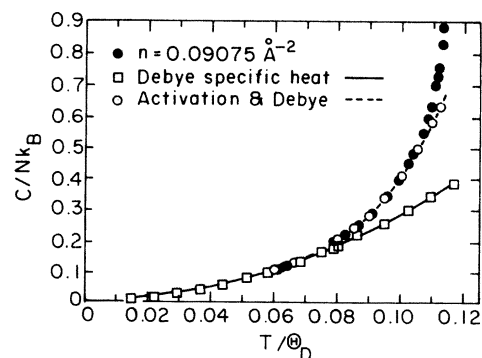


FIG. 11. Experimental specific heat compared to Debye model with constant Θ_D (—) and Debye solid plus defect activation (---).

zation of heterogeneity by vapor-pressure isotherms, but an estimate consistent with the measurements can be made.

A. Ideal specific heat for first-order melting

We do not know the precise characteristics of an ideal first-order melting peak but we can construct an approximate one from the experimental data. The specific-heat contribution far from the melting peak is assumed to have ideal single-phase properties. Ecke *et al.*¹⁹ showed that energy heterogeneity has a small effect on single-phase properties when the distribution of binding energies is fairly narrow and symmetric. We will assume that the behavior of the experimental specific heat outside a temperature interval of $T_{\text{peak}} \pm 0.2T_{\text{peak}}$ is that of an ideal single phase. The lower temperature corresponds to the end of the region described by the Debye plus defect contributions. The upper temperature is taken to be the same temperature increment above T_{peak} .

The low-temperature solid has been characterized below $T/\Theta_D \approx 0.10$ earlier in Sec. III. Above the melting transition the specific heat falls smoothly to a constant value (Fig. 2), with an increase in magnitude as T_{peak} is approached from above. (We neglect at this time the small subsidiary peak or shoulder seen at temperatures slightly higher than the peak.) This form is approximated as $C/Nk_B = 0.30 + 1.96/T$. An estimate of the specific-heat discontinuity is obtained from evaluating the expression for the conversion heat capacity in the two-phase region (see Appendix) at the solid phase boundary,

$$\frac{\Delta C}{Nk_B} = \frac{T}{nK_T} \left[\frac{1}{n} \frac{dn}{dT} \right]^2 \quad (8)$$

with the values for the compressibility of the solid, K_T , taken from Elgin and Goodstein's expression for the zero-temperatures 2D spreading pressure of ^4He on graphite,⁴

$$\phi = 5.5(10n)^6 + 0.81 \quad (9)$$

in units of dyn/cm. The liquid phase discontinuity is taken to be equal to the solid discontinuity since the compressibilities are comparable. At a density $n = 0.09 \text{ \AA}^{-2}$ and a transition temperature of about 3 K, the calculated discontinuity is $\Delta C/Nk_B = 1.2$. The compressibility close to melting is greater than the $T=0$ value, so this calculation sets an upper bound on the magnitude of the discontinuity. We note that as the coverage increases the discontinuity increases, due to the rapid dependence of the compressibility on density. This is consistent with the increase in height of the experimental specific-heat peaks.

The ideal width of the two-phase region is determined by the condition that total entropy of melting be the same for the ideal and experimental peaks. Since the width is broadened by heterogeneity, it is less than the full width at half maximum of the experimental peaks. The experimental widths range from 0.1 K at $n = 0.08933 \text{ \AA}^{-2}$ to 0.2 K at $n = 0.09388 \text{ \AA}^{-2}$. The ideal two-phase region is assumed to be symmetrically situated about T_{peak} and the ideal solid and liquid properties obtained earlier are extrapolated to the phase boundaries. The presumed ideal

first-order specific heat, constructed in this manner, is shown in Fig. 12.

B. Finite size

With the ideal specific heat calculated, the influence of heterogeneity can be quantified. The finite sizes of substrate crystallites and uniform domains lead to thermodynamic fluctuations and edge effects which will result in a smearing of the ideal behavior over a certain temperature interval.

Imry³⁴ has shown that the temperature width due to fluctuations is related to the entropy change in a first-order phase transition by

$$\frac{\Delta T}{T} \sim \frac{1}{Ns}, \quad (10)$$

where s equals entropy change per particle and N equals the number of particles in a uniform domain. Grafoil has a linear domain size^{35,36} of roughly 100 \AA , while the domain size for graphite foam^{22,37} is at least 300 \AA . For helium film densities of about 0.09 \AA^{-2} , these domain sizes give rise to particle numbers of 900 for Grafoil and 8100 for foam. The latent entropy of melting, in units of k_B , has been estimated to be from 0.03 for $n = 0.0893 \text{ \AA}^{-2}$ to 0.08 for $n = 0.0939 \text{ \AA}^{-2}$. Table IV shows the temperature broadening due to fluctuations for several densities with domain sizes corresponding to Grafoil and foam. On the basis of this comparison one can see that finite-size smearing due to fluctuations will be unimportant relative to the widths of the melting peaks (greater than 0.1 K) of ^4He /foam in the density range of $0.089\text{--}0.094 \text{ \AA}^{-2}$. At lower densities the decreasing latent heat will cause the smearing to be greater. In Grafoil, on the other hand, the temperature fluctuation of 0.12 K at $n = 0.09 \text{ \AA}^{-2}$ is about the same as the melting-peak widths and should play an important role in rounding the ideal specific-heat signal. This may be one of the reasons why the $0.0842\text{-}\text{\AA}^{-2}$ peak on foam is considerably sharper than the Grafoil peak at that density. At higher densities in Grafoil, the smearing is also reduced appreciably and should not be the dominant factor in rounding the transition.

In addition to finite-size rounding due to temperature fluctuations, there are effects due to the non-negligible

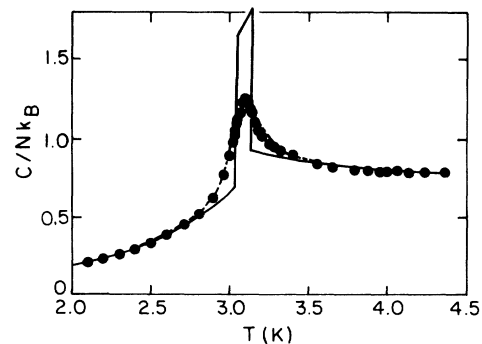


FIG. 12. Calculated specific heat of an ideal first-order transition (—), a heterogeneity-broadened first-order transition (---), and the experimental transition, for density $n = 0.09075 \text{ \AA}^{-2}$ (●).

TABLE IV. Calculated temperature broadening of first-order melting peaks due to temperature fluctuations in small domains.

n (\AA^{-2})	T (K)	s/k_B	$N=8100$		$N=900$	
			$\Delta T/T$	ΔT (K)	$\Delta T/T$	ΔT (K)
0.0893	2.78	0.03	0.004	0.01	0.04	0.12
0.0910	3.14	0.05	0.0025	0.008	0.02	0.06
0.0939	3.69	0.08	0.0015	0.006	0.01	0.04

edge-to-surface ratio of finite-size domains. The finite size causes a shift in chemical potential relative to an infinite system, given by³⁶

$$\delta\mu = \frac{\alpha_{ls}}{nr} \quad (11)$$

where α_{ls} is the liquid-solid line tension and r is the radius of the finite-size domain. The 2D line tension is estimated from the 3D surface tension as the surface tension in a single atomic layer of thickness L by $\alpha_{ls,2D} = L\alpha_{ls,3D}$. A 3D value³⁸ of 0.10 erg/cm^2 and a thickness of 3 \AA gives a 2D line tension of $3 \times 10^{-2} \text{ erg/cm}$. For Grafoil, $r \cong 50 \text{ \AA}$, while $r > 150 \text{ \AA}$ for graphite foam. The resultant shifts in chemical potential are 0.04 K for Grafoil and 0.01 K for foam. The temperature shift in the melting peak due to this variation in chemical potential is approximately

$$\delta T = \frac{dT}{dn} n^2 K_T \delta\mu. \quad (12)$$

With compressibilities calculated from Eq. (9), $k_B \delta T \cong 0.18 \delta\mu$ for densities close to 0.09 \AA^{-2} . The temperature shift is only 0.004 K for Grafoil and 0.001 K for foam. These temperature shifts are insignificant compared to the measured widths.

C. Energy heterogeneity

Another source of heterogeneity is the variation in substrate binding energy. Although no explicit calculation has been done for helium melting in the manner described by Ecke *et al.*,¹⁹ one can obtain estimates of the effects by scaling their results and by making reasonable assumptions about how the binding-energy variation depends on the substrate-adsorbate interaction.

We have characterized the heterogeneity of the foam graphite substrate with vapor-pressure isotherms of Kr and Xe, using the analysis of Dash and Puff.³⁹ By this procedure we obtain the distribution of binding energy of the test gases. The distributions are approximately Gaussian over the central regions, with halfwidths $\delta\epsilon = 4.5 \pm 1.5 \text{ K}$ for xenon and $\delta\epsilon = 2.5 \pm 0.5 \text{ K}$ for krypton. With binding energies of 2000 and 1800 K , respectively, fractional widths are $\delta\epsilon/\epsilon = 0.0025 \pm 0.0008$ and $\delta\epsilon/\epsilon = 0.0015 \pm 0.0003$. An average of these two widths, $\delta\epsilon/\epsilon \cong 0.002$, is taken as the magnitude of the binding-energy variation. The width of the variation in helium is estimated by scaling the width for krypton in the manner described by Dash and Puff,³⁹

$$\delta\epsilon_1/\epsilon_1 = \delta\epsilon_2/\epsilon_2, \quad (13)$$

where the subscripts 1 and 2 refer to different rare-gas ad-

sorbates. The binding energy of helium is about 140 K ,⁴⁰ so the scaled width in helium is $\delta\epsilon < 0.28 \text{ K}$. The resultant temperature halfwidth broadening, with the use of Eqs. (12) and (9), is $\delta T_{hw} < 0.02 \text{ K}$.

The use of Eq. (12) to estimate the temperature broadening of a first-order discontinuity due to variations in substrate binding energy is an approximation which ignores the specific-heat contribution due to the redistribution of the surface density. As the temperature changes, the film density changes on areas of the substrate with different binding energy. This redistribution requires energy in excess of the energy required to change the temperature of the film (see Dash and Puff³⁹). Thermal redistribution effects can be large for some transitions; for example, the liquid-vapor transition in the model system described by Ecke *et al.*¹⁹ is temperature broadened by 5 times as much as an estimate based on Eq. (12). In the high-density region, the effects of redistribution should be smaller due to the lower compressibilities of the solid and liquid. We estimate that the full widths including distribution are in the range $0.04 < \Delta T < 0.16 \text{ K}$.

To reproduce an averaged specific-heat peak from the ideal heat-capacity function presented in Sec. IV A, we assume a Gaussian distribution of transition temperatures for the central region, consistent with the krypton and xenon isotherms. Rather than a single Gaussian, we use a combination of Gaussians with widths σ_1 and σ_2 and weights w_1 and w_2 to approximate the tails of the measured distribution because the results of Ecke *et al.*¹⁹ indicate that the tails of the distribution are broader than the simple narrow Gaussian which describes most of the area. We convolute the ideal specific heat with the broadening function to obtain an averaged specific heat given by

$$\begin{aligned} \frac{\bar{C}}{Nk_B} = & w_1 \int_{-8\sigma_1}^{8\sigma_1} \frac{C_{ideal}(T_s, T)}{Nk_B} F(\bar{T}_s, T_s, \sigma_1) dT_s \\ & + w_2 \int_{-8\sigma_2}^{8\sigma_2} \frac{C_{ideal}(T_s, T)}{Nk_B} F(\bar{T}_s, T_s, \sigma_2) dT_s, \end{aligned} \quad (14)$$

where

$$F(\bar{T}_s, T_s, \sigma) = \frac{1}{\sigma\sqrt{2\pi}} e^{-[(\bar{T}_s - T_s)/\sigma]^2/2}, \quad (15)$$

and T_s is the solid phase-boundary temperature. The weights and widths of the distribution, the ideal heat-capacity discontinuity, the two-phase temperature width, and the solid phase-boundary temperature are adjusted to fit the experimental specific heat at $n = 0.09075 \text{ \AA}^{-2}$. The ideal and averaged curves are shown in Fig. 12 for the fitting parameters listed in Table V. Note that the fitted pa-

TABLE V. Parameters in calculation of averaged and ideal specific heat of ${}^4\text{He}/\text{foam}$. $\sigma_1, \sigma_2, W_1, W_2$, and T_s are described in the text in relation to Eq. (14). $\Delta C/Nk_B$ is the specific-heat discontinuity of the ideal first-order transition, and ΔT is the temperature width of the ideal phase boundary at constant density.

Parameter	σ_1 (K)	σ_2 (K)	W_1	W_2	$\Delta C/Nk_B$	T_s (K)	ΔT (K)
Estimated	0.02–0.08				< 1.2	3.05	< 0.15
Fitted	0.05	0.20	65%	35%	0.925	3.04	0.10

Parameters are all close to the estimates, with the possible exception of the fraction of the substrate with the larger temperature width. This fraction may not accurately reflect the wider portion of the binding-energy distribution because it is difficult to separate single-phase contributions to the specific heat from the effects of heterogeneity. Some of the increase in the experimental specific heat near the peak could be due to an increase in the single-phase specific heat and not due to a wider distribution of binding energies. Also, the effective distribution of transition temperatures is not the binding-energy distribution. The actual binding-energy distribution produces an effective distribution of transition temperatures through the averaging process. Since the averaging includes redistribution contributions to the specific heat, there is no reason to expect that the effective temperature distribution has exactly the same form as the binding-energy distribution.

While the calculation of the averaged specific heat is approximate, as noted earlier, the success in reproducing the experimental behavior raises the possibility that the transition is intrinsically first order, but experimentally broadened by variations in substrate binding energy. However, our analysis does not preclude a continuous transition, and this will be considered in the next section.

V. COMPARISONS

We have presented evidence that defects are excited in the low-temperature solid phase of ${}^4\text{He}$ adsorbed on graphite foam and that the experimental melting peaks are consistent with a first-order melting transition. In this section we will compare our results with the predictions of theories of 2D melting and with NMR, neutron scattering, and spreading pressure measurements.

The dislocation-mediated melting model of Kosterlitz, Thouless, Halperin, and Nelson^{14–16} makes definite predictions about the properties of the solid phase and the melting transition. The melting due to the unbinding of dislocation pairs is a continuous transition, with an essential singularity at T_m . At an essential singularity all thermodynamic derivatives are finite, so there is no divergence in the specific heat at T_m . A broad specific-heat peak due to the progressive unbinding of the remaining dislocation pairs would occur above T_m . Halperin and Nelson¹⁶ showed that if the melting transition is a continuous dislocation unbinding transition, the high-temperature phase retains some slowly decaying angular correlation. A second transition is necessary to destroy this intermediate phase, which Halperin and Nelson call the hexatic phase due to the hexagonal symmetry of the angular correlations. They showed that the second transition, due to the unbinding of disclination pairs, is also characterized by an

essential singularity.

Halperin and Nelson also considered the effects of a periodic potential on the properties of the melting transition. For the melting of an incommensurate film on a substrate with triangular symmetry (such as He/graphite), the hexatic phase is stabilized and no second transition due to disclination pair unbinding should occur.

Although Halperin and Nelson predict a two-stage continuous melting transition mediated by the unbinding of pairs of topological excitations, they do not rule out the possibility of a first-order transition preempting the higher-order transition. Chui¹⁷ proposed a grain-boundary mechanism for first-order melting, but others are also possible. In general, first-order melting occurs when the liquid free energy becomes less than the solid free energy. This may happen before the solid becomes unstable to the formation of particular microscopic defects. If the transition is first order, the melting temperature should be less than the temperature of unbinding of dislocation pairs.

We can compare the predicted dislocation melting temperatures with the ${}^4\text{He}/\text{graphite}$ specific-heat peak temperatures. If the melting transition is continuous as described by the dislocation model, then the calculated melting temperatures would lie below the peak temperatures. For first-order melting the calculated temperatures should be greater than the peak temperatures. The dislocation melting temperature T_m , in terms of the Lamé elastic constants μ and λ of the solid, is¹⁶

$$T_m = \frac{a_0^2}{4\pi k_B} \frac{\mu(\mu + \lambda)}{(2\mu + \lambda)}, \quad (16)$$

where a_0 is the lattice constant. By relating the elastic properties to the Debye temperature at $T=0$ K, one can obtain an approximate expression for T_m in terms of Θ_D , by assuming the Cauchy condition, $\mu = \lambda$ (Ref. 41):

$$T_m = \frac{mk_B}{8h^2} \left[\frac{\Theta_D^2}{n} \right]. \quad (17)$$

Previous comparisons^{2,4,42,43} have utilized Eq. (17) and the experimentally determined Debye temperatures because of a lack of information about the elastic constants. However, the approximation required to obtain Eq. (17) neglects several important effects. The first is the assumption of the Cauchy condition on the Lamé coefficients. The second is the neglect of the finite pressure required to stabilize the helium solid. Stewart⁴⁴ has shown that the initial pressure modifies the relationship of the elastic and thermal parameters needed to calculate Eq. (17) from Eq. (16). There is also a correction to the melting tempera-

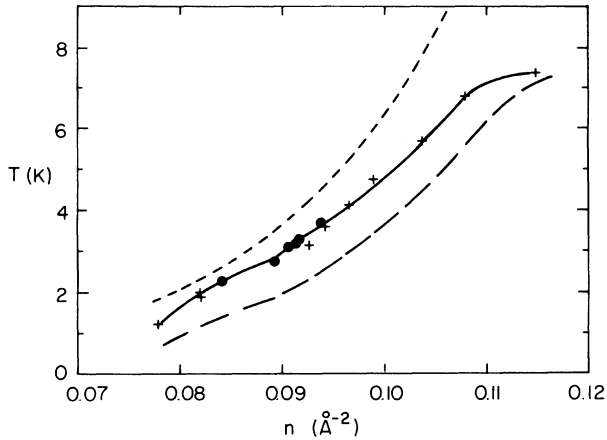


FIG. 13. Comparison of specific-heat peak temperatures for ${}^4\text{He}/\text{foam}$ and ${}^4\text{He}/\text{Grafoil}$ with calculated Kosterlitz-Thouless melting temperatures T_m . Experimental peak temperatures (—); T_m , from Eq. (17) and experimental Debye temperatures (---); T_m , from Eq. (18) and elastic constants from Goodstein and Greif (Ref. 24) (-.-).

tures due the orientational influence of the substrate. The dislocation melting temperature of a 2D solid film with a periodic substrate potential is¹⁶

$$T_m^c = \frac{a_0^2}{4\pi k_B} \left[\frac{\mu(\mu + \lambda)}{(2\mu + \lambda)} + \frac{\mu\gamma}{\mu + \lambda} \right], \quad (18)$$

where γ is the elastic constant which measures the resistance to rotation of the overlayer lattice with respect to the substrate. Goodstein and Greif²⁴ have calculated the elastic properties of ${}^4\text{He}$, taking into account initial stress and substrate influences. With the use of their values for μ , λ , and γ , the dislocation melting temperatures for ${}^4\text{He}/\text{graphite}$ can be calculated from Eq. (18). Figure 13 shows a graph of the calculated T_m and the heat-capacity peak temperatures. Note that the T_m values calculated from Eq. (17) are considerably less than those obtained from Eq. (18). The substrate correction is less than 5%, so the primary difference is due to the Cauchy approximation and the neglect of the finite-pressure correction in Eq. (17).

There is another effect which influences the calculated melting temperatures. The elastic constants in Eqs. (16) and (18) should be evaluated at the melting temperature. As a first approximation, the temperature dependence of the elastic constants can be estimated from computer-simulation studies. The combination of elastic constants, which enters into the formulas for the melting temperatures, is $\mu(\mu + \lambda)/(2\mu + \lambda)$. In the computer study of Tobochnik and Chester⁴⁵ this combination decreases by about 10% between $0.6T_m$ and T_m , including the effects of renormalization near T_m . This decreases the values of T_m calculated above. However, the dislocation melting temperatures, which are calculated to lie 20% above the experimental peak temperatures when the temperature dependence of the elastic constants is neglected, are still above the peak temperatures when this effect is included. Although this result is consistent with a first-order transi-

tion preempting the dislocation melting mechanism, better measurement or calculation of the temperature dependence of the elastic constants for helium is needed before the effect can be accurately assessed.

Numerous studies^{18,29,30} of 2D melting have been made employing computer-simulation techniques. Some results have been interpreted as indicating first-order melting,^{18,30,46,47} but others have shown evidence for continuous melting.^{45,48,49} The order of the melting transition may be difficult to determine from computer simulations because there are finite-size and finite-time limitations which make the interpretation of the results uncertain.^{30,49,50} For temperatures below the melting region, the studies agree qualitatively on the properties of the solid. There is evidence for the thermal activation of defects, including dislocation pairs and grain-boundary loops, with activation energies of about $10k_B T_m$ (Refs. 29 and 45) and defect concentrations of about 5%.²⁹

Saito⁵¹ finds that for a group of interacting dislocation pairs on a triangular lattice the order of the transition depends on the dislocation core energy. For high core energy, he finds a continuous transition while for a 30% lower core energy the transition is first order, characterized by a large discontinuous increase in the defect concentration at melting.

Several of the theoretical and computer calculations have generated specific-heat peaks which can be compared to the experimental curves. Our experimental peaks have widths of $\delta T/T = 0.08$. Values for three different specific-heat calculations are as follows: (1) $\delta T/T = 0.2$, Saito,⁵¹ vector-dislocation model (Monte Carlo); (2) $\delta T/T = 0.27$, Solla *et al.*,⁵² scalar XY model (renormalization group); (3) $\delta T/T = 0.35$, Tobochnik and Chester,⁵³ scalar XY model (Monte Carlo). The calculated curves are broader than the experimental peak even though the experimental curve is broadened by energy heterogeneity. However, the calculated peaks are nonuniversal. A more rapid unbinding of dislocation pairs due to a smaller core energy could produce a narrower peak but that would increase the defect concentration at melting and tend to favor a first-order transition if Saito's arguments are correct. The defect concentration at the critical temperature for the XY model, closely related to the dislocation melting model, is 0.3%,⁵² which is close to the defect concentrations at melting for the specific-heat data (Table II). This indicates that the core energies are comparable and that a large decrease in the calculated width of the peak in the XY model would require a core energy much smaller than the experimentally determined core energy for helium.

The specific-heat analysis of Sec. III A indicates that vacancies (or tightly bound dislocation pairs) are thermally excited in ${}^4\text{He}$ below the melting temperature with activation energies that agree with the NMR results of Richards⁹ and Owers-Bradley.³² The NMR results of Widom *et al.*,⁴³ which showed a frequency-dependent relaxation time, are interpreted by them as indicating a Halperin-Nelson transition from solid to hexatic liquid crystal. The temperatures of the onset of the frequency-dependent relaxation time correspond closely to the temperatures at which the NMR measurements detected the

beginning of vacancy activation (Table VI). The specific-heat data indicate the onset of appreciable activation at $T/\Theta_D=0.08$ for densities close to 0.09 \AA^{-2} . The ^3He NMR reduced onset temperature for $n=0.0896 \text{ \AA}^{-2}$ is $T/\Theta_D=0.083$. We believe that this correlation of the onset temperatures of the frequency-dependent relaxation time with the activation onset temperatures of the NMR and specific-heat data indicates that the frequency dependence of the relaxation time is a consequence of the thermal activation and not due to a dislocation melting transition as suggested by Richards *et al.*

The neutron scattering results of Lauter *et al.*^{8,33} show a decrease in the lattice constant a_0 of solid ^3He /Grafoil close to melting. At $n=0.0910 \text{ \AA}^{-2}$, a_0 remains constant up to 3 K. From 3 to 4.1 K, there is a decrease of about 1.0% in a_0 . Several factors could be responsible for this decrease. The activation of vacancies causes an increase in pressure in the solid and a resultant decrease in a_0 . Lauter *et al.*³³ found that an activation energy of 40 K, an activation entropy of $5.1k_B$, and a vacancy area of unity could explain the decrease in lattice constant over the entire range from 3 to 4.1 K. However, the solid melts at 3.8 K as evidenced by the specific-heat peak of Hering *et al.*² Also, the activation parameters obtained from specific heat of ^4He /foam (Table II) and from NMR data of ^3He /Grafoil (Table VI) are significantly less than the values obtained by Lauter *et al.* If the melting is first order, an increase in temperature at constant coverage causes a decrease in the solid lattice spacing because there is a rapid increase in pressure in the two-phase coexistence region. The magnitude of the decrease in lattice spacing due to an increase in pressure is given by

$$\frac{\delta a_0}{a_0} = \frac{1}{a_0} \frac{\partial a_0}{\partial n} \frac{\partial n}{\partial \phi} \delta \phi = -\frac{1}{2} K_T \delta \phi. \quad (19)$$

From the spreading pressure measurements of Hurlbut⁵⁴ for ^4He /graphite, $\delta \phi \cong 0.18 \text{ dyn/cm}$, while $K_T \cong 0.05 \text{ cm/dyn}$ from Eq. (9). The fractional change in a_0 is 0.5%. Since close to melting K_T is larger than its value at $T=0 \text{ K}$, the fractional change is somewhat greater than 0.5%.

With the use of the specific-heat parameters and a vacancy area of $a_v/a \cong 0.7$ consistent with the spreading pressure measurements of Hurlbut, the decrease in a_0 due to thermal activation of defects is 0.3% at 3.8 K. The decrease in lattice spacing due to both vacancy and first-order melting contributions is $\delta a_0/a_0 \cong 0.8\%$ at 4 K, in

approximate agreement with the neutron scattering results.

The diffuse secondary specific-heat peak that is visible for the coverage $n=0.08933 \text{ \AA}^{-2}$ and the changes in the density dependence of Θ_D , C_{peak} , and T_{peak} close to that coverage remain to be considered. The second peak could be interpreted as the transition due to the loss of orientational epitaxy in the fluid phase, described by Halperin.⁵⁵ He pointed out that if the incommensurate solid phase has two favored orientation angles and if that orientation is not destroyed by the initial transition, then a second transition might occur at higher temperature between this oriented liquid and the hexatic liquid phase. This transition should have Ising-type behavior with the two Ising states being the two angular orientations of the liquid. Goodstein and Greif²⁴ showed that 2D solid helium does have such angles of orientation. They calculated an angle of 22° for ^4He at $n=0.092 \text{ \AA}^{-2}$ and $T=0 \text{ K}$ with an orientation energy per atom of 0.07 K. ^3He at the same density has about the same angle but an energy of only 0.02 K. There are several reasons to associate the diffuse peak with orientational epitaxy. First, the change in the density dependence of Θ_D , C_{peak} , and T_{peak} occurs close to the density, $n=0.09 \text{ \AA}^{-2}$. This is near the density where the diffuse peak occurs in the specific heat and is also about the density that the maximum value of the rotational elastic constant of ^4He /graphite, calculated by Goodstein and Grief, occurs. Also, the change in the density dependence of the Debye temperatures indicates that the effect is associated with the structure of the solid. The correlation of these properties suggests that the diffuse second peak, the change in slope of the phase boundary and the changes in the density dependence of the Debye temperatures near 0.09 \AA^{-2} are due to orientational epitaxy.

VI. CONCLUSIONS

Our results are consistent with past experimental studies of the ^4He /Grafoil in the behavior of the solid film, however, several new results have been obtained in the current work. Evidence for vacancy (or dislocation pair) activation is seen in the specific-heat data, helping to explain the low-temperature behavior in the NMR experiments of Richards⁹ and others.^{32,42} We have shown that the melting transition is consistent with a first-order transition broadened by a fractional variation of substrate binding energy of $\delta\epsilon/\epsilon \cong 3.4 \times 10^{-4}$. The interpretation

TABLE VI. Activation energy, activation onset temperature, and onset temperature of frequency-dependent relaxation time from NMR measurements.^{9,32} T_{fd} (K) is the onset temperature of frequency-dependent relaxation time.

Fractional coverage	$n \text{ (\AA}^{-2}\text{)}$	$u_a/k_B \text{ (K)}$	$T_{\text{act}} \text{ (K)}$ ($\pm 2 \text{ K}$)	$T_{\text{fd}} \text{ (K)}$ ($\pm 0.2 \text{ K}$)
0.765	0.0826	11	1.2	1.06(0.2)
0.80	0.0864	16	1.75	1.96(0.08)
0.83	0.0896	21	2.55	2.44(0.12)
0.88	0.0950	27	3.30	3.28(0.1)
0.92	0.0990	35	4.10	4.08(0.2)
0.96	0.104	42	4.95	4.88(0.25)

that the melting transition of $^4\text{He}/\text{graphite}$ is first order is also consistent with the neutron scattering results of Lauter *et al.*^{8,33} Furthermore, the predicted dislocation melting temperatures are greater than the specific-heat peak temperatures, implying first-order melting. However, despite the agreement of the experimental data and the theoretical arguments, we have not proven that the transition is first order. Additional measurements are necessary before a decision between the two alternatives can be made.

On the basis of the current study, we propose a modified $^4\text{He}/\text{graphite}$ phase diagram, Fig. 14. We believe that the 1-K peaks reported by Hering *et al.*² represent a triple line where registered, incommensurate solid and fluid coexist. Hering *et al.* also observed broad peaks close to 2.5 K which we attribute to the registered-fluid phase boundary. Our estimate of the pure fluid density at the triple point is $n=0.075 \text{ \AA}^{-2}$. The experimental triple line is curved, with a maximum temperature at the pure fluid point due to a combination of energy heterogeneity and finite-size effects. The details of such effects are not known, but the basic mechanisms seem to offer the best explanation for this region of the helium phase diagram. If the melting transition is first order, the coexistence region has a density width of about 0.0005 \AA^{-2} and a temperature width of about 0.1 K except near the triple line where it widens to 0.003 \AA^{-2} and 0.5 K. At $n \cong 0.09 \text{ \AA}^{-2}$, the diffuse peak above the much sharper melting peak, Figs. 3 and 4, combined with the break in the slope of the melting line, signals some new behavior. The dif-

fuse peak above the melting peak may be due to remnant orientational epitaxy in the hexatic fluid after melting. As discussed in Sec. V, a second transition may occur above T_m if the orientation of the film is not destroyed by melting. The underlying hexagonal symmetry of the substrate can stabilize the fluid and may also stabilize the orientational epitaxy of that phase. Clearly more work needs to be done, exploring this characteristic of the ^4He film. Theoretical work on the phase transition associated with the loss of orientational epitaxy and on the properties of 2D melting on a structured substrate might be helpful in understanding these questions. Also, new specific-heat measurements with the use of better graphite substrate could reveal more of the details of the second peak.

ACKNOWLEDGMENTS

We wish to thank R. D. Puff and S. Solla for many useful discussions. This work was supported in part by the National Science Foundation, under Grant No. DMR-81-16421.

APPENDIX

In Sec. IV we calculated the specific-heat discontinuity at a first-order phase boundary from Eq. (8). This is an exact formula which can be derived from the expression for the total heat capacity in the two-phase region.

The total entropy S_{total} is the sum of the single-phase entropies, S_1 and S_2 . Similarly, the total particle number and surface area are given by $N=N_1+N_2$ and $A=A_1+A_2$. The total entropy per unit area is $s=S_{\text{total}}/A=s_1(A_1/A)+s_2(A_2/A)$. The area fraction of atoms in phase 1, x , is A_1/A . In terms of the number densities of the phases $x=(n_2-n)/(n_2-n_1)$, where $n=N/A$. So the expression for the areal entropy in terms of the single-phase contributions is

$$s = xs_1 + (1-x)s_2 \quad (\text{A1})$$

The heat capacity per area, $c=C/A=T(ds/dT)_n$, follows from Eq. (A1):

$$c = xT \left[\frac{ds_1}{dT} \right]_{n_1} + (1-x)T \left[\frac{ds_2}{dT} \right]_{n_2} + T(s_1-s_2) \frac{dx}{dT} + T \left[\frac{\partial s_1}{\partial n_1} \right]_T \frac{dn_1}{dT} + T \left[\frac{\partial s_2}{\partial n_2} \right]_T \frac{dn_2}{dT} \quad (\text{A2})$$

The first two terms are the single-phase contributions to the total heat capacity per unit area. The remaining terms represent the conversion contributions. From now on we will just consider the conversion part of the total heat capacity,

$$\frac{c_{\text{conv}}}{T} = (s_1-s_2) \frac{dx}{dT} + \left[\frac{\partial s_1}{\partial n_1} \right]_T \frac{dn_1}{dT} + \left[\frac{\partial s_2}{\partial n_2} \right]_T \frac{dn_2}{dT} \quad (\text{A3})$$

From the Gibbs-Duhem relation, $n d\mu = -s dT + d\phi$ and the Clausius-Clapeyron equation

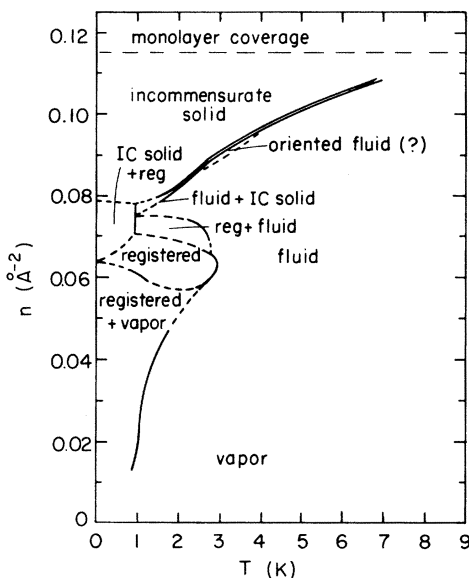


FIG. 14. Proposed phase diagram of $^4\text{He}/\text{graphite}$. The solid lines (—) represent regions where the data are adequate to determine the phase boundary. The dashed lines (---) indicate our conjectured phase boundaries. The line of experimental peaks at 1 K is curved slightly, but we have displayed the triple line as occurring at constant temperature as it would in the ideal film. The curvature in the real film is thought to be due to heterogeneous effects.

$$\frac{d\phi}{dT} = \frac{n_2 s_1 - n_1 s_2}{n_2 - n_1}, \quad (\text{A4})$$

one gets

$$\frac{d\mu}{dT} = \frac{s_1 - s_2}{n_2 - n_1}. \quad (\text{A5})$$

Using this expression and the relation $(\partial s/\partial n)_T = s/n - \alpha/nK_T$, where α is the thermal expansion coefficient and K_T is the isothermal compressibility, we get

$$C_{\text{conv}} = x \left[\frac{s_1}{n_1} - \alpha_1 K_{T_1} + \frac{d\mu}{dT} \right] \frac{dn_1}{dT} + (1-x) \left[\frac{s_2}{n_2} - \alpha_2 K_{T_2} + \frac{d\mu}{dT} \right] \frac{dn_2}{dT}. \quad (\text{A6})$$

Finally one can show that $s/n - \alpha/nK_T + d\mu/dT = (dn/dT)/n^2 K_T$, which yields

$$\frac{C_{\text{conv}}}{T} = \frac{x}{KT_1} \left[\frac{1}{n_1} \frac{dn_1}{dT} \right]^2 + \frac{1-x}{KT_2} \left[\frac{1}{n_2} \frac{dn_2}{dT} \right]^2. \quad (\text{A7})$$

- ¹M. Bretz, J. G. Dash, D. C. Hickernell, E. O. McLean, and O. E. Vilches, *Phys. Rev. A* **8**, 1589 (1973).
- ²S. Hering, S. W. Van Sciver, and O. E. Vilches, *J. Low Temp. Phys.* **25**, 793 (1976); S. Hering, Ph.D. thesis, University of Washington, Seattle, 1974 (unpublished).
- ³D. C. Hickernell, E. O. McLean, and O. E. Vilches, *J. Low Temp. Phys.* **23**, 789 (1976).
- ⁴R. L. Elgin and D. L. Goodstein, *Phys. Rev. A* **9**, 2657 (1974).
- ⁵M. J. Tejwani, O. Ferreira, and O. E. Vilches, *Phys. Rev. Lett.* **44**, 152 (1980); M. J. Tejwani, Ph.D. thesis, University of Washington, Seattle, 1979 (unpublished).
- ⁶K. Carneiro, W. Ellenson, L. Passell, J. P. McTague, and H. Taub, *Phys. Rev. Lett.* **37**, 1695 (1976).
- ⁷M. Nielsen, J. P. McTague, and W. Ellenson, *J. Phys. (Paris) Suppl.* **10**, C-4, 10 (1977).
- ⁸H. J. Lauter, H. Wiechert, and R. Feile, in *Ordering in Two Dimensions*, edited by S. K. Sinha (North-Holland, New York, 1980), p. 291.
- ⁹For a review of NMR studies, see M. Richards, in *Phase Transitions in Surface Films*, edited by J. G. Dash and J. Ruvalds (Plenum, New York, 1980), p. 165.
- ¹⁰D. C. Hickernell, D. L. Husa, and J. G. Daunt, *Phys. Rev. Lett.* **49**, 435 (1974).
- ¹¹G. Boato, P. Cantini, and R. Tatarek, *Phys. Rev. Lett.* **40**, 887 (1978).
- ¹²R. Elgin, in *Proceedings of the 13th International Conference of Low Temperature Physics*, edited by K. D. Timmerhaus, W. J. O'Sullivan, and E. F. Hammel (University of Colorado Press, Boulder, Colorado, 1973), p. 175.
- ¹³G. A. Stewart, S. Siegel, and D. L. Goodstein, in *Proceedings of the 13th International Conference of Low Temperature Physics*, edited by K. D. Timmerhaus, W. J. O'Sullivan, and E. F. Hammel (University of Colorado, Boulder, Colorado, 1973), p. 181.
- ¹⁴M. Kosterlitz and D. Thouless, *J. Phys. C* **6**, 1181 (1975).
- ¹⁵R. Feynman (unpublished); see R. L. Elgin and D. L. Goodstein, in *Monolayer and Submonolayer Helium Films*, edited by J. G. Daunt and E. Lerner (Plenum, New York, 1973), p. 35.
- ¹⁶D. R. Nelson and B. I. Halperin, *Phys. Rev. B* **19**, 2457 (1979).
- ¹⁷S. I. Chui, *Phys. Rev. Lett.* **48**, 933 (1982).
- ¹⁸For a review and bibliography of computer simulations, see F. Abraham, *Phys. Rep.* **80**, 339 (1980).
- ¹⁹R. E. Ecke, J. G. Dash, and R. D. Puff, *Phys. Rev. B* **26**, 1288 (1982).
- ²⁰CryoCal, Inc., 2457 University Ave., St. Paul, MN, Model No. CR1000.
- ²¹J. S. Walker, M. Schick, and M. Wortis, *Phys. Rev. B* **16**, 2205 (1977).
- ²²M. Bienfait, J. G. Dash, and J. Stoltenberg, *Phys. Rev. B* **21**, 2765 (1980).
- ²³J. S. Dugdale and F. E. Simon, *Proc. R. Soc. London Ser. A* **218**, 291 (1953).
- ²⁴D. L. Goodstein and J. Greif, *J. Low Temp. Phys.* **44**, 347 (1981).
- ²⁵For a description of 2D lattice dynamics on a triangular lattice, see P. Dean, *Proc. Cambridge Philos. Soc.* **59**, 383 (1963).
- ²⁶H. R. Glyde, in *Rare Gas Solids*, edited by M. L. Klein and J. A. Venables (Academic, New York, 1977), Vol. 1, Chap. 7.
- ²⁷C. A. Swenson, in *Rare Gas Solids*, edited by M. L. Klein and J. A. Venables (Academic, New York, 1977), Vol. 2, p. 877.
- ²⁸A. V. Chadwick and H. R. Glyde, in *Rare Gas Solids*, edited by M. L. Klein and J. A. Venables (Academic, New York, 1977), Vol. 2, p. 1157.
- ²⁹J. P. McTague, D. Frenkel, and M. P. Allen, in *Ordering in Two Dimensions*, edited by S. K. Sinha (North-Holland, New York, 1980), p. 147.
- ³⁰J. Broughton, G. Gilmer, and J. Weeks, *Phys. Rev. B* **25**, 4651 (1982).
- ³¹D. Fisher, R. Morf, and B. I. Halperin, *Phys. Rev. B* **20**, 4692 (1979).
- ³²J. R. Owers-Bradley, Ph.D. thesis, University of Sussex, England, 1978 (unpublished).
- ³³H. Lauter, H. Wiechert, and R. Feile, *Phys. Rev. B* **25**, 3410 (1982).
- ³⁴Y. Imry, *Phys. Rev. B* **21**, 2042 (1980).
- ³⁵J. K. Kjems, L. Passell, H. Taub, J. G. Dash, and A. D. Novaco, *Phys. Rev. B* **13**, 1446 (1976).
- ³⁶T. T. Chung and J. G. Dash, *Surf. Sci.* **66**, 559 (1977).
- ³⁷R. J. Birgeneau, P. A. Heiney, and J. P. Pelz, in *Proceedings of the 16th International Conference on Low-Temperature Physics [Physica B + C 109&110]*, 1785 (1982).
- ³⁸S. Balibar, D. O. Edwards, and C. Larouche, *Phys. Rev. Lett.* **42**, 782 (1979).
- ³⁹J. G. Dash and R. D. Puff, *Phys. Rev. B* **24**, 295 (1981).
- ⁴⁰M. W. Cole, D. R. Frankl, and D. L. Goodstein, *Rev. Mod. Phys.* **53**, 199 (1980).
- ⁴¹A. Novaco, *J. Low Temp. Phys.* **9**, 457 (1972).
- ⁴²The Cauchy condition, $\mu = \lambda$, is assumed in the discussion of J. M. Kosterlitz and D. J. Thouless, in *Progress in Low Temperature Physics*, edited by D. F. Brewer (North-Holland, New York, 1978), Vol. 7B, p. 417.
- ⁴³A. Widom, J. R. Owers-Bradley, and M. G. Richards, *Phys. Rev. Lett.* **29**, 1340 (1979).
- ⁴⁴G. A. Stewart, *Phys. Rev. A* **10**, 671 (1974).
- ⁴⁵J. Tobochnik and G. V. Chester, in *Ordering in Two Dimensions*, edited by S. K. Sinha (North-Holland, New York,

- 1980), p. 339.
- ⁴⁶F. F. Abraham, *Phys. Rev. B* **23**, 6145 (1981).
- ⁴⁷J. Phillips, L. Bruch, and R. Murphy, *J. Chem. Phys.* **75**, 5097 (1981).
- ⁴⁸D. Frenkel and J. P. McTague, *Phys. Rev. Lett.* **42**, 1632 (1979).
- ⁴⁹A. D. Novaco and P. Shea, *Phys. Rev. B* **26**, 284 (1982).
- ⁵⁰M. Fisher and D. Huse (unpublished) based on closing remarks of M. E. Fisher at Ninth Midwest Solid State Theory Symposium on Melting, Localization and Chaos, Argonne National Laboratory, Argonne, Illinois, 1982 (in press).
- ⁵¹Y. Saito, *Phys. Rev. Lett.* **48**, 1114 (1982).
- ⁵²S. Solla and E. Riedel, *Phys. Rev. B* **23**, 6008 (1981).
- ⁵³J. Tobochnik and G. V. Chester, *Phys. Rev. B* **20**, 3761 (1979).
- ⁵⁴S. Hurlbut (private communication).
- ⁵⁵B. I. Halperin, in *Ordering in Two Dimensions*, edited by S. K. Sinha (North-Holland, New York, 1980), p. 143.